

# Holographic p-wave superfluid in Gauss-Bonnet gravity

Shancheng Liu<sup>1,2</sup>, Qiyuan Pan<sup>1,2\*</sup> and Jiliang Jing<sup>1,2†</sup>

<sup>1</sup> *Department of Physics, Key Laboratory of Low Dimensional Quantum Structures and Quantum Control of Ministry of Education, Hunan Normal University, Changsha, Hunan 410081, China and*

<sup>2</sup> *Synergetic Innovation Center for Quantum Effects and Applications, Hunan Normal University, Changsha, Hunan 410081, China*

## Abstract

We construct the holographic p-wave superfluid in Gauss-Bonnet gravity via a Maxwell complex vector field model and investigate the effect of the curvature correction on the superfluid phase transition in the probe limit. We obtain the rich phase structure and find that the higher curvature correction hinders the condensate of the vector field but makes it easier for the appearance of translating point from the second-order transition to the first-order one or for the emergence of the Cave of Winds. Moreover, for the supercurrents versus the superfluid velocity, we observe that our results near the critical temperature are independent of the Gauss-Bonnet parameter and agree well with the Ginzburg-Landau prediction.

PACS numbers: 11.25.Tq, 04.70.Bw, 74.20.-z

---

\* panqiyuan@126.com

† jljing@hunnu.edu.cn

## I. INTRODUCTION

In recent years, the anti-de Sitter/conformal field theories (AdS/CFT) correspondence, which can connect a strongly correlated system in a  $d$ -dimensional flat spacetime with a  $(d + 1)$ -dimensional asymptotic AdS spacetime [1–3], has been used to provide some meaningful theoretical insights in order to understand the mechanism of the high temperature superconductors from the gravitational dual [4]; for reviews, see Refs. [5–8] and references therein. It was found that the so-called holographic superconductor model, which admits black holes with scalar hair at low temperatures (superconducting phase) but without scalar hair at high temperatures (normal phase), turns out to be quite successful in giving the qualitative features of the s-wave superconductivity [9, 10]. Introducing an  $SU(2)$  Yang-Mills field into the bulk, where a gauge boson generated by one  $SU(2)$  generator is dual to the vector order parameter, the authors of Ref. [11] presented a holographic realization of p-wave superconductivity. Interestingly, Ref. [12] constructed a new holographic p-wave superconductor model by introducing a charged vector field into an Einstein-Maxwell theory with a negative cosmological constant, which is a generalization of the  $SU(2)$  model with a general mass and gyromagnetic ratio [13]. In Refs. [14, 15], the holographic d-wave superconductivity was realized by introducing a charged massive spin two field propagating in the bulk.

The aforementioned works on the gravitational dual models of the superconductorlike transition focus on the vanishing spatial components of the  $U(1)$  gauge field on the AdS boundary. Since the supercurrent in superconducting materials is very important in condensed matter systems, it is worthwhile to construct the corresponding holographic superfluid models by turning on the spatial components of the gauge field according to the AdS/CFT correspondence. Performing a deformation of the superconducting black hole, i.e., turning on a spatial component of the gauge field that only depends on the radial coordinate, the authors of Refs. [16, 17] constructed a holographic superfluid solution and found that the second-order superfluid phase transition can change to the first order when the velocity of the superfluid component increases relative to the normal component. Areal *et al.* studied the phases of the s-wave holographic superfluids and observed the Cave of Winds phase structure where the system first suffers a second-order transition and then a first-order phase transition when the temperature decreases [18]. Extending the investigation to the holographic p-wave superfluid model in the AdS black holes coupled to a Maxwell complex vector field, Wu *et al.* showed that the translating superfluid velocity from second order to first order increases with the increase of the mass squared

of the vector field and the Cave of Winds takes place only in the five-dimensional spacetime [19]. Interestingly, in Ref. [20] the authors obtained that the Cave of Winds appears in some range of the Lifshitz parameter even in the four-dimensional spacetime. Other generalized investigations based on the holographic superfluid model can be found, for example, in Refs. [21–30].

As a further step along this line, it is of great interest to generalize the investigation on the holographic superfluid model to the Gauss-Bonnet gravity [31] and investigate the effect of the curvature correction on the superfluid phase transition, which will help us to understand systematically the influences of the  $1/N$  or  $1/\lambda$  ( $\lambda$  is the 't Hooft coupling) corrections on the holographic dual models. It was observed that the higher curvature correction makes the condensate of holographic superconductors harder to form and causes the behavior of the claimed universal ratio  $\omega/T_c \approx 8$  unstable [32, 33], which is motivated by the application of the Mermin-Wagner theorem to the holographic superconductors. Rich phenomena in the phase transition were also found for the holographic superconductors in the Gauss-Bonnet gravity where the Gauss-Bonnet parameter can play the role in determining the order of phase transition and critical exponents in the second order phase transition [34, 35]. Considering the increasing interest in study of the Gauss-Bonnet dual models [36–49] and holographic p-wave models via the Maxwell complex vector field model [12, 13], in this work we are going to examine the influence of the curvature correction on the holographic p-wave superfluid model which has not been constructed as far as we know. We will find that the Gauss-Bonnet correction affects not only the condensate of the vector field but also the appearance of transition point from the second-order transition to the first-order one or the emergence of the Cave of Winds. However, near the critical temperature, the ratio  $(\langle O_x \rangle_c / \langle O_x \rangle_\infty)^2 = 2/3$ , which is independent of the Gauss-Bonnet correction. For simplicity and clarity, we will concentrate on the probe limit where the backreaction of matter fields on the spacetime metric is neglected.

The structure of this work is as follows. In Sec. II we will construct the holographic p-wave superfluid model with the Gauss-Bonnet corrections in the probe limit. In particular, we derive the equations of motion and the grand potential for the superfluid model in the Gauss-Bonnet gravity. In Sec. III we will consider the rich phase structure of the system and investigate the effect of the curvature correction on the superfluid phase transition. In Sec. IV we will explore the effect of the curvature correction on the supercurrents versus superfluid velocity. We will conclude in the last section with our main results.

## II. DESCRIPTION OF THE HOLOGRAPHIC DUAL SYSTEM

In order to construct the Gauss-Bonnet holographic p-wave model of superfluidity in the probe limit, we start with the five-dimensional AdS black hole in the Gauss-Bonnet gravity in the form [31]

$$ds^2 = -r^2 f(r) dt^2 + \frac{dr^2}{r^2 f(r)} + r^2 (dx^2 + dy^2 + dz^2), \quad (1)$$

with

$$f(r) = \frac{1}{2\alpha} \left[ 1 - \sqrt{1 - \frac{4\alpha}{L^2} \left( 1 - \frac{r_+^4}{r^4} \right)} \right], \quad (2)$$

where  $L$  is the AdS radius,  $r_+$  is the black hole horizon and  $\alpha$  is the Gauss-Bonnet parameter with the upper bound, i.e., the Chern-Simons limit  $\alpha = L^2/4$ . Note that there are the constraints of the causality via the holographic correspondence [50, 51], we will take the range  $-7L^2/36 \leq \alpha \leq 9L^2/100$  for the Gauss-Bonnet parameter in this work. In the asymptotic region ( $r \rightarrow \infty$ ), we have

$$f(r) \sim \frac{1}{2\alpha} \left( 1 - \sqrt{1 - \frac{4\alpha}{L^2}} \right), \quad (3)$$

so the effective asymptotic AdS scale can be defined by [31]

$$L_{\text{eff}}^2 = \frac{2\alpha}{1 - \sqrt{1 - \frac{4\alpha}{L^2}}}. \quad (4)$$

Obviously, the metric (1) will reduce to the Schwarzschild AdS case when  $\alpha \rightarrow 0$ . The Hawking temperature of the black hole, which will be interpreted as the temperature of the CFT, can be determined by

$$T = \frac{r_+}{\pi L^2}. \quad (5)$$

For convenience, we will scale  $L = 1$  in the following calculation.

Considering the Maxwell complex vector field model [12, 13], we will build the holographic p-wave model of superfluidity in the Gauss-Bonnet AdS black hole background via the action

$$S = \frac{1}{16\pi G} \int d^5x \sqrt{-g} \left( -\frac{1}{4} F_{\mu\nu} F^{\mu\nu} - \frac{1}{2} \rho_{\mu\nu}^\dagger \rho^{\mu\nu} - m^2 \rho_\mu^\dagger \rho^\mu + iq\gamma \rho_\mu \rho_\nu^\dagger F^{\mu\nu} \right), \quad (6)$$

where we have defined  $F_{\mu\nu} = \nabla_\mu A_\nu - \nabla_\nu A_\mu$  and  $\rho_{\mu\nu} = D_\mu \rho_\nu - D_\nu \rho_\mu$  with the covariant derivative  $D_\mu = \nabla_\mu - iqA_\mu$ .  $\rho_\mu$  is the complex vector field with mass  $m$  and charge  $q$ . It should be noted that the last term, which describes the interaction between the vector field  $\rho_\mu$  and the gauge field  $A_\mu$ , will not play any role since we study the case without external magnetic field in this work.

Adopting the following ansatz for the matter fields

$$\rho_\mu dx^\mu = \rho_x(r)dx, \quad A_\mu dx^\mu = A_t(r)dt + A_y(r)dy, \quad (7)$$

where both a time component  $A_t$  and a spatial component  $A_y$  of the vector potential have been introduced in order to consider the possibility of DC supercurrent, we will obtain the equations of motion in the probe limit

$$\rho_x'' + \left(\frac{3}{r} + \frac{f'}{f}\right) \rho_x' - \frac{1}{r^2 f} \left(m^2 + \frac{q^2 A_y^2}{r^2} - \frac{q^2 A_t^2}{r^2 f}\right) \rho_x = 0, \quad (8)$$

$$A_t'' + \frac{3}{r} A_t' - \frac{2q^2 \rho_x^2}{r^4 f} A_t = 0, \quad (9)$$

$$A_y'' + \left(\frac{3}{r} + \frac{f'}{f}\right) A_y' - \frac{2q^2 \rho_x^2}{r^4 f} A_y = 0, \quad (10)$$

where the prime denotes the derivative with respect to  $r$ . From the above equations of motion, one can easily demonstrate that the complex vector field model is still a generalization of the  $SU(2)$  Yang-Mills model in the holographic superfluid model even in the Gauss-Bonnet gravity, which supports the argument given in [13, 19]. On the other hand, Eqs. (8) and (9) reduce to the case considered in [49] for the holographic p-wave conductor/superconductor phase transition in the Gauss-Bonnet gravity, where the spatial component  $A_y$  has been turned off.

We will count on the shooting method [9, 10] to solve numerically the equations of motion with the appropriate boundary conditions. At the event horizon  $r = r_+$ , the regularity condition gives

$$A_t(r_+) = 0, \quad \rho_x'(r_+) = \frac{1}{r_+^2 f'(r_+)} \left[ m^2 + \frac{q^2 A_y^2(r_+)}{r_+^2} \right] \rho_x(r_+), \quad A_y'(r_+) = \frac{2q^2 \rho_x^2(r_+)}{r_+^4 f'(r_+)} A_y(r_+). \quad (11)$$

At the asymptotic AdS boundary  $r \rightarrow \infty$ , we have asymptotic behaviors

$$\rho_x = \frac{\rho_{x-}}{r^{\Delta_-}} + \frac{\rho_{x+}}{r^{\Delta_+}}, \quad A_t = \mu - \frac{\rho}{r^2}, \quad A_y = S_y - \frac{J_y}{r^2}, \quad (12)$$

where  $\Delta_\pm = 1 \pm \sqrt{1 + m^2 L_{\text{eff}}^2}$  is the characteristic exponent,  $\mu$  and  $S_y$  are the chemical potential and superfluid velocity, while  $\rho$  and  $J_y$  are the charge density and current in the dual field theory, respectively. Note that  $\rho_{x-}$  and  $\rho_{x+}$  are interpreted as the source and the vacuum expectation value of the vector operator  $\langle O_x \rangle$  in the dual field theory according to the AdS/CFT correspondence, we will impose boundary condition  $\rho_{x-} = 0$  since we require that the condensate appears spontaneously.

Interestingly, from the equations of motion (8)-(10) we can get the useful scaling symmetries and the transformation of the relevant quantities

$$\begin{aligned} r \rightarrow \lambda r, \quad (t, x, y, z) &\rightarrow \frac{1}{\lambda} (t, x, y, z), \quad q \rightarrow q, \quad (\rho_x, A_t, A_y) \rightarrow \lambda (\rho_x, A_t, A_y), \\ (T, \mu, S_y) &\rightarrow \lambda (T, \mu, S_y), \quad (\rho, J_\varphi) \rightarrow \lambda^3 (\rho, J_\varphi), \quad \rho_{x+} \rightarrow \lambda^{1+\Delta} \rho_{x+}, \end{aligned} \quad (13)$$

to build the invariant and dimensionless quantities. For simplicity, we use the scaling symmetries to set  $r_+ = 1$  and  $q = 1$  when performing numerical calculations.

On the other hand, we can obtain important information about the phase transition of the system from the behavior of the grand potential  $\Omega = -T\mathcal{S}_{os}$  of the bound state, where  $\mathcal{S}_{os}$  is the Euclidean on-shell action. As in Refs. [16–20], we still work in the grand canonical ensemble since we can fix the chemical potential by considering the scaling symmetries and the transformation (13). From the action (6), we get

$$\begin{aligned}\mathcal{S}_{os} &= \frac{1}{16\pi G} \int dt dx dy dz dr \sqrt{-g} \left[ -\frac{1}{2} \nabla_\mu (A_\nu F^{\mu\nu}) - \nabla_\mu (\rho_\nu^\dagger \rho^{\mu\nu}) + \frac{1}{2} A_\nu \nabla_\mu F^{\mu\nu} \right] \\ &= \frac{V_3}{16\pi GT} \left( -\frac{1}{2} \sqrt{-\gamma} n_r A_\nu F^{r\nu} \Big|_{r \rightarrow \infty} - \sqrt{-\gamma} n_r \rho_\nu^\dagger \rho^{r\nu} \Big|_{r \rightarrow \infty} + \frac{1}{2} \int_{r_+}^{\infty} dr \sqrt{-g} A_\nu \nabla_\mu F^{\mu\nu} \right) \\ &= \frac{V_3}{16\pi GT} \left[ \mu\rho - \frac{S_y J_y}{L_{\text{eff}}^2} + \int_{r_+}^{\infty} dr \frac{\rho_x^2}{r} \left( A_y^2 - \frac{A_t^2}{f} \right) \right],\end{aligned}\tag{14}$$

where we have used the integration  $\int dt dx dy dz = V_3/T$ . It should be noted that we do not need to introduce the Gibbons-Hawking boundary term for the well-defined Dirichlet variational problem and the counterterms for the divergent terms in the on-shell action since we neglect the backreaction of matter fields on the spacetime metric and impose the source-free boundary condition [19, 20]. Ignoring the prefactor  $16\pi G$  for simplicity, we can express the grand potential in the superfluid phase as

$$\frac{\Omega_S}{V_3} = -\frac{T\mathcal{S}_{os}}{V_3} = -\mu\rho + \frac{S_y J_y}{L_{\text{eff}}^2} + \int_{r_+}^{\infty} dr \frac{\rho_x^2}{r} \left( \frac{A_t^2}{f} - A_y^2 \right).\tag{15}$$

Considering that  $\rho_x = 0$  in the normal phase, we can easily obtain the grand potential in this case

$$\frac{\Omega_N}{V_3} = -\mu^2.\tag{16}$$

### III. CONDENSATES OF THE VECTOR FIELD

In this section, we will numerically solve the system of coupled differential equations (8)-(10) and obtain the condensate  $\langle O_x \rangle$  as a function of the temperature and the superfluid velocity. In order to determine the critical temperature and which phase is more thermodynamically favored, we also calculate the grand potential  $\Omega$  of the bound state.

Before studying the condensed phase with nonzero  $A_y$ , we first review the results of the conductor/superconductor phase transition with  $A_y = 0$  in [49]. It is clearly shown that, in the absence of the superfluid velocity, the holographic conductor/superconductor phase transition is always the second-order one [49]. In Fig. 1, we exhibit the critical temperature  $T_c$  as a function of the Gauss-Bonnet parameter  $\alpha$  for the

fixed mass of the vector field  $m^2 L_{eff}^2 = -3/4, 0, 5/4$  and  $3$ . Obviously, the critical temperature decreases as the Gauss-Bonnet parameter increases, which indicates that the increasing high curvature correction hinders the conductor/superconductor phase transition. Interestingly, this conclusion is independent of the mass of the vector field. Our results agree well with the findings in the Gauss-Bonnet gravity for the p-wave condensates in the Maxwell complex vector field model [49] and Yang-Mills theory [38], and the s-wave condensates [32, 33].

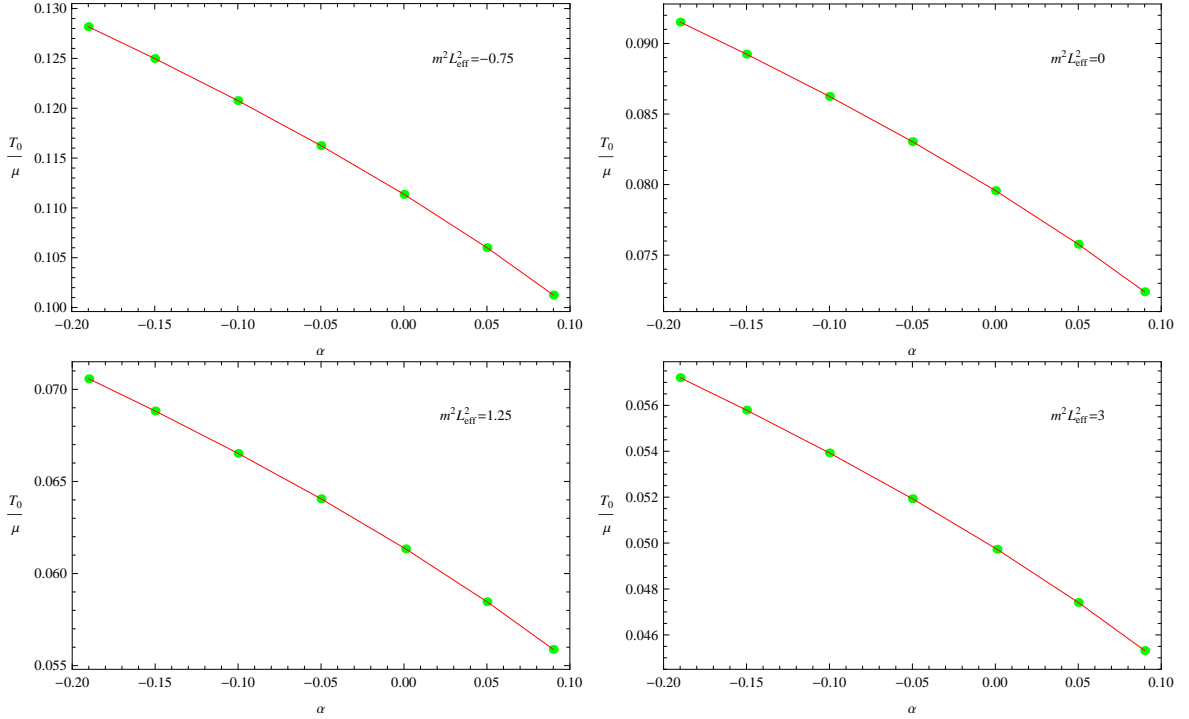


FIG. 1: (Color online) The critical temperature  $T_0$  without the superfluid velocity as a function of the Gauss-Bonnet parameter  $\alpha$  for the fixed mass of the vector field  $m^2 L_{eff}^2 = -3/4, 0, 5/4$  and  $3$ .

Now we are in a position to study the effects of the Gauss-Bonnet parameter on the phase transition with superfluid velocity. In Ref. [18], the authors found that the phase structure of the s-wave superfluid model in the 5D AdS black hole depends on the range of the scalar mass, i.e., for small mass beyond the BF bound, the phase transition changes from the second order to the first order when the superfluid velocity increases to the translating value; for the intermediate mass scale, the Cave of Winds appears; and for sufficiently high mass, the phase transition is always of the second order, no matter how high the superfluid velocity. The holographic p-wave superfluid models in the 5D AdS black hole [19] and 4D Lifshitz black hole [20] coupled to a Maxwell complex vector field share similar features for the condensates of the vector field. Thus, we will present our results in an appropriate range of the vector field mass.

As an example of the small mass scale, we give in Fig. 2 the condensate and the corresponding grand

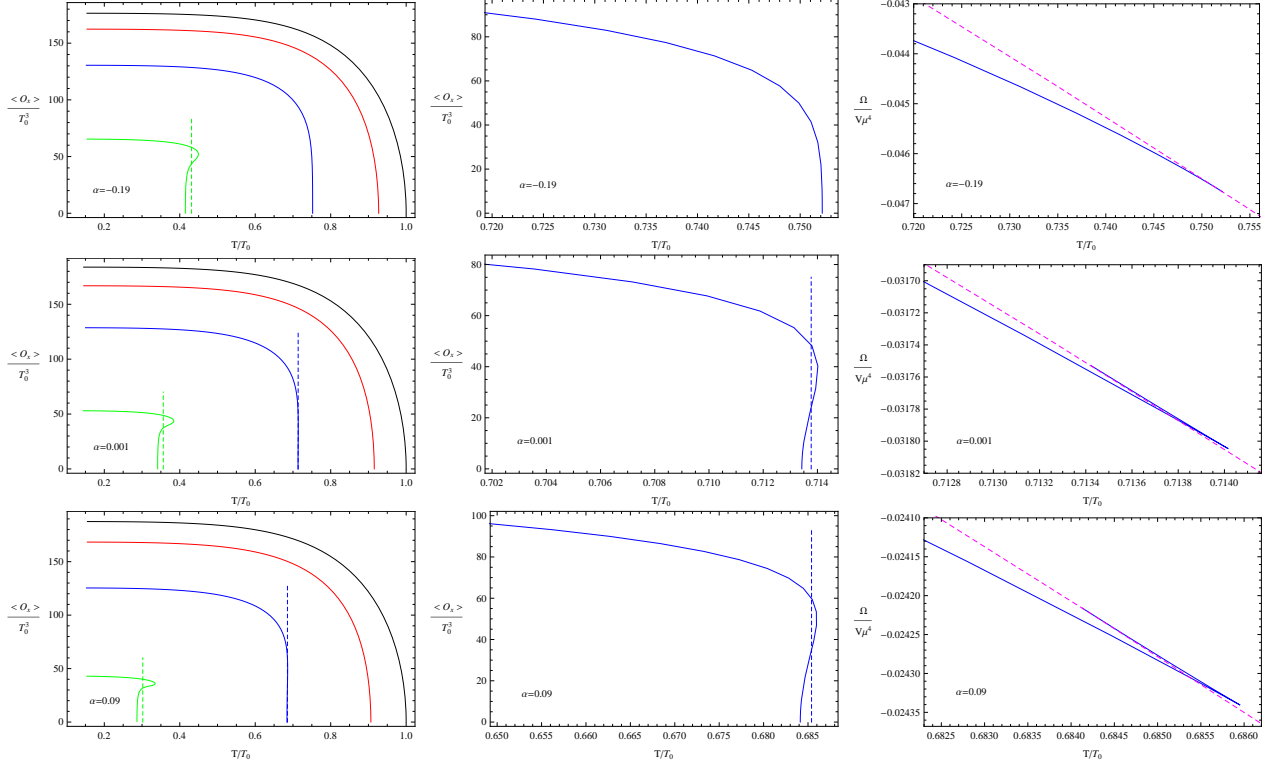


FIG. 2: (Color online) The condensate and the grand potential as a function of the temperature with the fixed mass of the vector field  $m^2 L_{eff}^2 = 0$  for different values of the Gauss-Bonnet parameter  $\alpha$ . For the left three panels, the four lines in each panel from top to bottom correspond to increasing superfluid velocity, i.e.,  $\frac{S_y}{\mu} = 0$  (black), 0.25 (red), 0.46 (blue) and 0.75 (green) respectively. For the middle three panels, the line in each panel corresponds to the superfluid velocity  $\frac{S_y}{\mu} = 0.46$  and a vertical line represents the critical temperature of the first-order phase transition. For the right three panels, the two lines in each panel correspond to the superfluid velocity  $\frac{S_y}{\mu} = 0.46$  (blue solid) and the normal phase (magenta dotted) respectively.

potential as a function of the temperature with  $m^2 L_{eff}^2 = 0$  for different values of  $\alpha$ . In the case of vanishing or small superfluid velocity, for example  $\frac{S_y}{\mu} = 0$  and 0.25 with  $\alpha = 0.001$ , the second-order phase transition occurs as the temperature is lowered below a critical value, where the critical temperature  $T_0$  with  $S_y = 0$  is given in Fig. 1. The second-order superfluid phase transition will change to the first order when superfluid velocity increases, for example  $\frac{S_y}{\mu} = 0.46$  and 0.75 with  $\alpha = 0.001$ , which is the result we can clearly observe from the grand potential with the typical swallowtails in the bottom two panels of the rightmost column in Fig. 2. Obviously, there exists a translating value of  $\frac{S_y}{\mu}$  beyond which the phase transition changes from the second order to the first order. In Fig. 3, we plot the translating superfluid velocity  $S_y/\mu$  from the second to the first order as a function of the Gauss-Bonnet parameter  $\alpha$  with  $m^2 L_{eff}^2 = 0$  and find that it almost decreases monotonously with  $\alpha$ , which shows that the higher curvature correction makes it easier for the emergence of the translating point. On the other hand, we mark the locations of the critical temperature with a vertical dotted line in the same color as the condensate curve for the first-order phase transition in Fig. 2.



It is found that the critical temperature decreases with the increase of the Gauss-Bonnet parameter, which indicates that the higher curvature correction hinders the condensate of the vector field even in the case of the first-order phase transition.

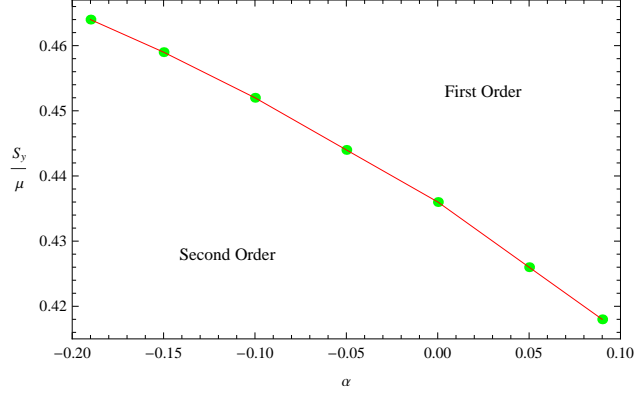


FIG. 3: (Color online) The translating superfluid velocity  $S_y/\mu$  from the second to the first order as a function of the Gauss-Bonnet parameter  $\alpha$  with the fixed mass of the vector field  $m^2 L_{eff}^2 = 0$ .

In the case of the intermediate mass, such as  $m^2 L_{eff}^2 = 5/4$ , we plot the condensate and the grand potential as a function of the temperature for different values of  $\alpha$  in Fig. 4. For the vanishing or small superfluid velocity, for example  $\frac{S_y}{\mu} = 0$  and  $0.50$  with  $\alpha = 0.001$ , the transition is second order and the condensate approaches zero as  $\langle O_x \rangle \sim (T_c - T)^\beta$  with the mean field critical exponent  $\beta = 1/2$  for all values of  $\alpha$ . However, when the superfluid velocity improves beyond a special value, we observe that  $\langle O_x \rangle$  becomes multivalued and the Cave of Winds appears, for example  $\frac{S_y}{\mu} = 0.70$  and  $0.80$  with  $\alpha = 0.001$ . The thermodynamically favored region of the Cave of Winds can be determined via its grand potential, just as in the bottom two panels of the middle and rightmost columns in Fig. 4. Fixing  $\frac{S_y}{\mu} = 0.70$ , from Fig. 4 we find that the transition is second order in the case of  $\alpha = -0.19$  but the Cave of Winds appears in the case of  $\alpha = 0.001$  or  $\alpha = 0.09$ , which shows that the higher curvature correction makes it easier for the emergence of the Cave of Winds. As a matter of fact, the other choices of the intermediate mass will not modify our result. This result seems to be interesting since we can control the emergence of the Cave of Winds by using the Gauss-Bonnet parameter. On the other hand, we also can see clearly from Fig. 4 that the critical temperature decreases with the increase of the Gauss-Bonnet parameter, which indicates that the higher curvature correction hinders the phase transition even the existence of the Cave of Winds.

Moving to the case of the sufficiently high mass, for example  $m^2 L_{eff}^2 = 3$ , we present in Fig. 5 the condensate and the corresponding grand potential as a function of the temperature for different values of  $\alpha$ . It should be noted that, even in the rather high superfluid velocity  $\frac{S_y}{\mu} = 0.80$ , the phase transition of the

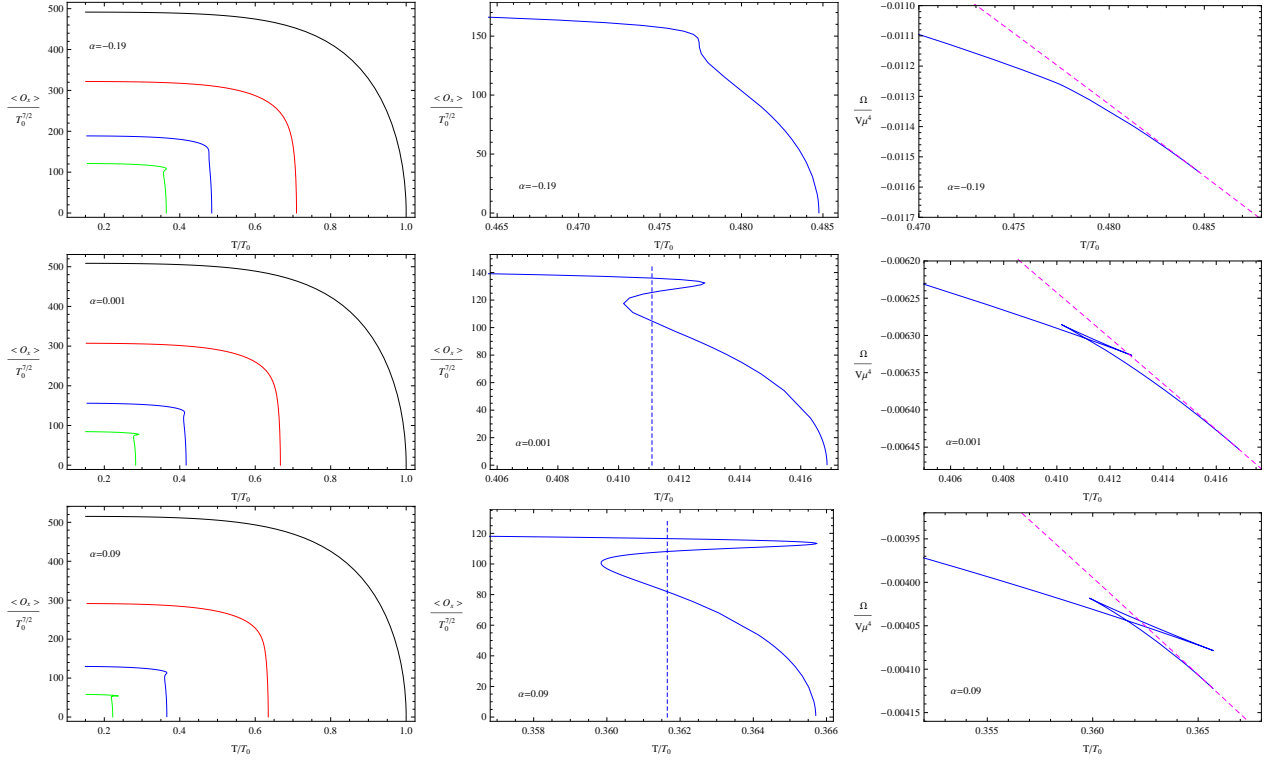


FIG. 4: (Color online) The condensate and the grand potential as a function of the temperature with the fixed mass of the vector field  $m^2 L_{eff}^2 = 5/4$  for different values of the Gauss-Bonnet parameter  $\alpha$ . For the left three panels, the four lines in each panel from top to bottom correspond to increasing superfluid velocity, i.e.,  $\frac{S_y}{\mu} = 0$  (black), 0.50 (red), 0.70 (blue) and 0.80 (green) respectively. For the middle three panels, the line in each panel corresponds to the superfluid velocity  $\frac{S_y}{\mu} = 0.70$  and a vertical line represents the thermodynamically stable bound of the Cave of Winds. For the right three panels, the two lines in each panel correspond to the superfluid velocity  $\frac{S_y}{\mu} = 0.70$  (blue solid) and the normal phase (magenta dotted) respectively.

system always belongs to the second order and the Gauss-Bonnet parameter can not change the order of phase transitions, which is consistent with the corresponding grand potential in the three panels of the right column in Fig. 5. Since the effect of  $\frac{q^2 A^2}{r^2}$  becomes relatively so weak that it can be ignored for a high enough mass even in the Gauss-Bonnet gravity, our results can be used to back up the findings obtained in Refs. [18, 19] that the system always suffers the second-order phase transition in the case of a sufficiently high mass.

#### IV. SUPERCURRENTS VERSUS THE SUPERFLUID VELOCITY

As the effective field theory of superconductors near the critical temperature  $T_c$ , Ginzburg-Landau (GL) theory can give an accurate description of such physical system and present various significant quantities that can directly be compared with the experimental results. Thus, we will study the relation between the supercurrent and the superfluid velocity in this section and then compare with GL theory.

In Fig. 6, we plot the supercurrent as a function of the superfluid velocity with the fixed mass of the

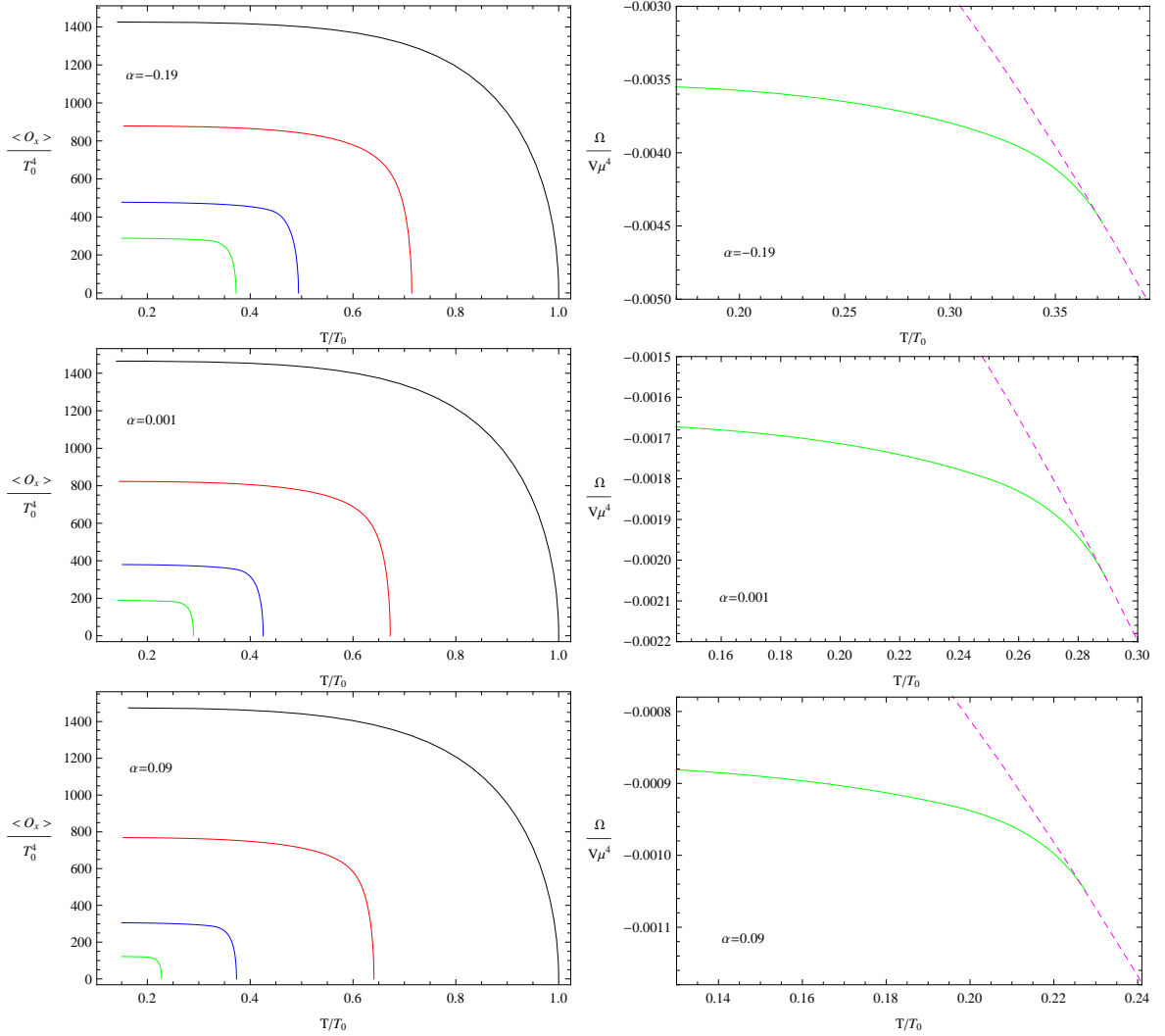


FIG. 5: (Color online) The condensate and the grand potential as a function of the temperature with the fixed mass of the vector field  $m^2 L_{eff}^2 = 3$  for different values of the Gauss-Bonnet parameter  $\alpha$ . For the left three panels, the four lines in each panel from top to bottom correspond to increasing superfluid velocity, i.e.,  $\frac{S_y}{\mu} = 0$  (black), 0.5 (red), 0.70 (blue) and 0.80 (green) respectively. For the right three panels, the two lines in each panel correspond to the superfluid velocity  $\frac{S_y}{\mu} = 0.80$  (green solid) and the normal phase (magenta dotted) respectively.

vector field  $m^2 L_{eff}^2 = 0, 5/4$  and  $3$  for different values of the Gauss-Bonnet parameter  $\alpha$ . Due to the rich phenomena in the phase transition, we have to discuss the behavior of the supercurrent in an appropriate range of the vector field mass. For small mass beyond the BF bound in the top three panels of Fig. 6, near the critical temperature, i.e.,  $T/T_0 = 0.98$ , for all values of the Gauss-Bonnet parameter  $\alpha$  considered here, it is observed that the curves approximate a parabola opening downward and the maximum value of the supercurrent denoted by  $\frac{J_y M_{ax}}{\mu^3}$  decreases with the increasing  $\alpha$ . At the intersecting point of the larger superfluid velocity with the abscissa axis, i.e.,  $\frac{S_y M_{ax}}{\mu}$ , we find that the supercurrent  $\frac{J_y}{\mu^3}$  decreases smoothly to zero, which indicates that the phase transition of the system belongs to the second order. This result is in

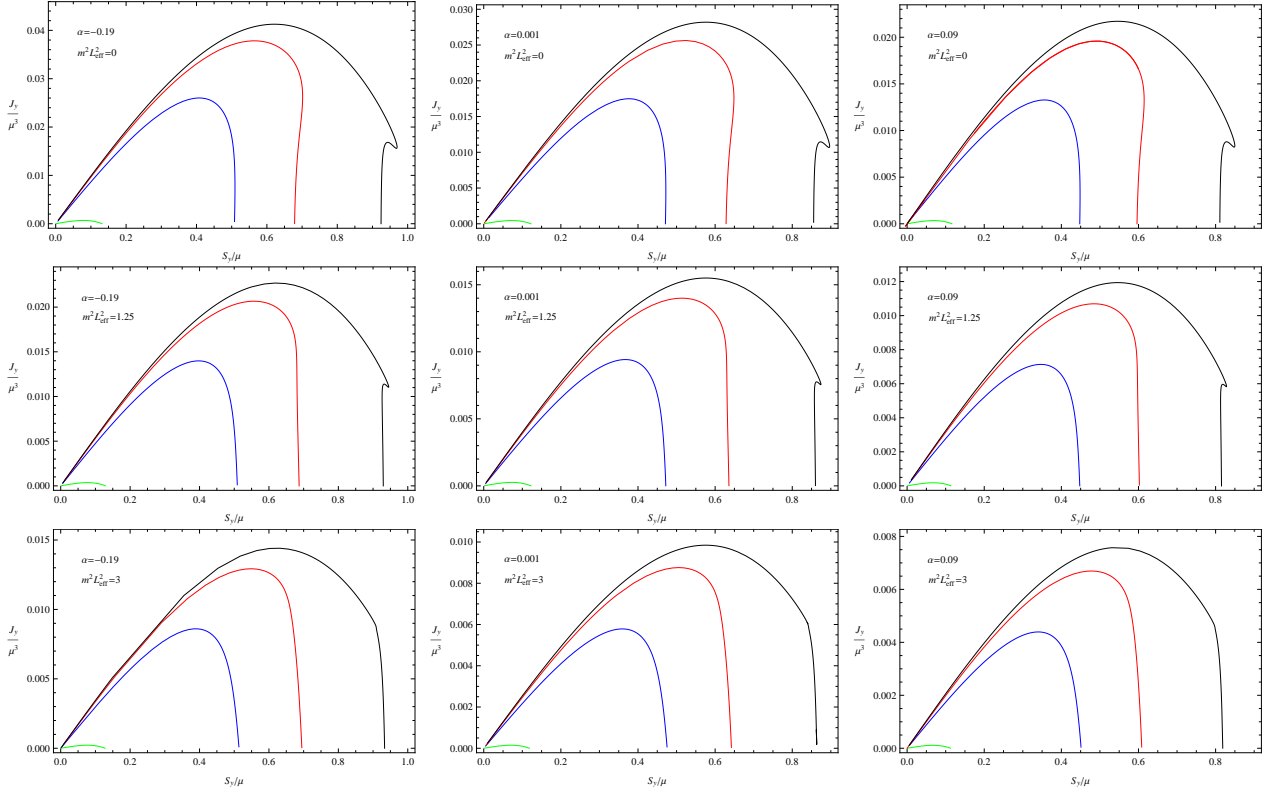


FIG. 6: (Color online) The supercurrent versus superfluid velocity with the fixed mass of the vector field for different values of the Gauss-Bonnet parameter  $\alpha$ . In each panel, the four lines from right to left correspond to  $T/T_0 = 0.2$  (black), 0.5 (red), 0.7 (blue) and 0.98 (green) respectively.

good agreement with the findings in the previous section and also the same as that of GL theory. When the temperature evidently deviates from the critical temperature, for example  $T/T_0 = 0.70$ , the linear dependence of the supercurrent on the superfluid velocity becomes more obvious until its maximum value  $\frac{J_y M \alpha x}{\mu^3}$ , which agrees well with the one in the thin superconducting films [52]. When the superfluid velocity increases and the temperature decreases to a certain value, such as  $T/T_0 = 0.50$  and  $0.2$ , the supercurrent versus the superfluid velocity becomes double valued, which implies the latent heat and the first-order phase transition in accordance with the results in Fig. 2. Especially, the larger the Gauss-Bonnet parameter  $\alpha$ , the more easy it is for the curve of the supercurrent to become double valued, which supports the findings of Fig. 3 and indicates that the higher curvature correction makes it easier for the emergence of the translating superfluid velocity from the second-order to the first-order phase transition. For the intermediate mass in the middle three panels of Fig. 6, near the critical temperature ( $T/T_0 = 0.98$ ), the relation between the supercurrent and the superfluid velocity is similar to the one in the case of  $m^2 L_{eff}^2 = 0$ , i.e., the curve of supercurrent versus superfluid approximates a parabola opening downward and the phase transition is of the second order. Decreasing the temperature goes over a value, for example  $T/T_0 = 0.20$ , we see clearly that the system first

suffers a second-order transition and then a first-order phase transition, but the critical point decreases as the Gauss-Bonnet parameter increases, which is consistent with the findings of Fig. 4 and means that the higher curvature correction makes it easier for the emergence of the Cave of Winds. For a high enough mass in the bottom three panels of Fig. 6, the holographic superfluid phase transition always belongs to the second order at the temperatures considered here, which is independent of the Gauss-Bonnet parameter  $\alpha$  and in good agreement with the results in Fig. 5. On the other hand, we also find that the higher curvature correction or larger mass, the lower the maximum value of the supercurrent  $\frac{J_{yMax}}{\mu^3}$ , which agrees well with the results in the previous section and suggests that the higher curvature correction or larger mass makes it harder for the holographic superfluid phase transition to be triggered.

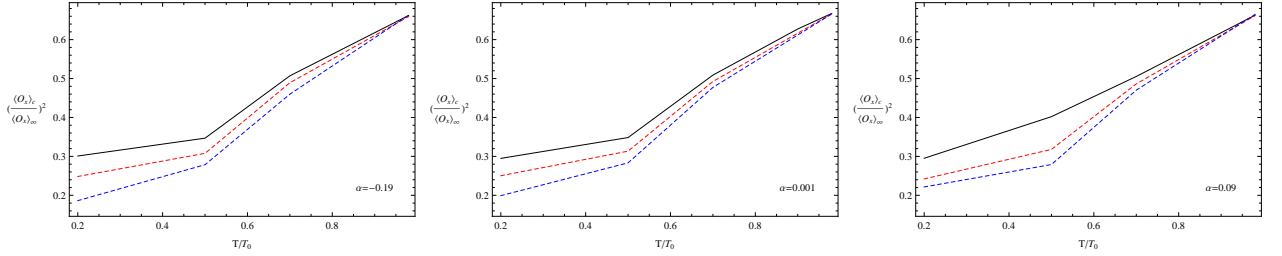


FIG. 7: (Color online) The ratio  $(\langle O_x \rangle_c / \langle O_x \rangle_\infty)^2$  versus the temperature with the fixed value of the Gauss-Bonnet parameter  $\alpha$  for different masses of the vector field. In each panel, the three lines from top to bottom correspond to  $m^2 L_{eff}^2 = 0$  (black),  $5/4$  (red) and  $3$  (blue) respectively.

In order to check the reasonability of our holographic model further, we will compare our results with another prediction of the GL theory

$$\left( \frac{\langle O_x \rangle_c}{\langle O_x \rangle_\infty} \right)^2 = \frac{2}{3}, \quad (17)$$

where  $\langle O_x \rangle_\infty$  and  $\langle O_x \rangle_c$  are defined as the values of the condensate corresponding to the vanishing superfluid velocity and the one with  $\frac{J_{yMax}}{\mu^3}$ , respectively. Calculating the ratio  $(\langle O_x \rangle_c / \langle O_x \rangle_\infty)^2$  in our holographic p-wave superfluid model with Gauss-Bonnet correction, we give the results with the fixed value of the Gauss-Bonnet parameter  $\alpha$  for different masses of the vector field, i.e.,  $m^2 L_{eff}^2 = 0, 5/4$  and  $3$  in Fig. 7. From panels we observe that, near the critical temperature, the ratio  $(\langle O_x \rangle_c / \langle O_x \rangle_\infty)^2$  is in very good agreement with GL theory for all cases considered here, which is independent of the Gauss-Bonnet parameter  $\alpha$ . However, the ratio deviates more evidently from the predicted value  $2/3$  when the temperature decreases gradually from the critical temperature and the mass increases from its BF bound. Interestingly, we observe that the difference caused by the mass of the vector field is reduced when the Gauss-Bonnet parameter becomes larger.

## V. CONCLUSIONS

In order to understand the influences of the  $1/N$  or  $1/\lambda$  ( $\lambda$  is the 't Hooft coupling) corrections on the holographic dual models, we have constructed the holographic p-wave superfluid model in the Gauss-Bonnet gravity via a Maxwell complex vector field model and obtained the effect of the curvature correction on the superfluid phase transition in the probe limit. We observed that, regardless of the superfluid velocity and the vector field mass, the critical temperature decreases as the Gauss-Bonnet parameter increases, which indicates that the higher curvature correction hinders the condensate of the vector field. It should be noted that this conclusion still holds even in the case of the first-order phase transition or the existence of the Cave of Winds. Considering the rich phase structure of this system, we found that for the small mass scale, the larger the Gauss-Bonnet parameter, the smaller the translating superfluid velocity becomes, which shows that the higher curvature correction makes it easier for the appearance of translating point from the second-order transition to the first-order one and implies that the Gauss-Bonnet parameter can change the order of the phase transition in the holographic p-wave superfluid system. In the case of the intermediate mass, we also noted that the higher curvature correction makes it easier for the emergence of the Cave of Winds. However, for the sufficiently high mass, we showed that the phase transition of the system always belongs to the second order and the Gauss-Bonnet parameter will not affect the order of phase transitions. Furthermore, we investigated the relation between the supercurrent and the superfluid velocity, which is consistent with the findings obtained from the condensates of the vector field in this model. In addition, we pointed out that, near the critical temperature, the ratio  $(\langle O_x \rangle_c / \langle O_x \rangle_\infty)^2$  agrees well with the GL theory, which is independent of the Gauss-Bonnet parameter. However, the ratio deviates much more obviously as the temperature decreases and the mass increases further. We found that the difference in ratio caused by the mass of the vector field is reduced when the Gauss-Bonnet parameter becomes larger. The extension of this work to the fully backreacted spacetime would be interesting since the backreaction provides richer physics in the Maxwell complex vector field model [12, 13]. We will leave it for further study.

## Acknowledgments

We thank Dr. Jun-Wang Lu for his helpful discussions. This work was supported by the National Natural Science Foundation of China under Grant Nos. 11275066 and 11475061; Hunan Provincial Natural Science

Foundation of China under Grant No. 2016JJ1012.

- 
- [1] J. Maldacena, Adv. Theor. Math. Phys. **2**, 231 (1998) [Int. J. Theor. Phys. **38**, 1113 (1999)].
  - [2] S.S. Gubser, I.R. Klebanov, and A.M. Polyakov, Phys. Lett. B **428**, 105 (1998).
  - [3] E. Witten, Adv. Theor. Math. Phys. **2**, 253 (1998).
  - [4] S.S. Gubser, Phys. Rev. D **78**, 065034 (2008).
  - [5] S.A. Hartnoll, Class. Quant. Grav. **26**, 224002 (2009).
  - [6] C.P. Herzog, J. Phys. A **42**, 343001 (2009).
  - [7] G.T. Horowitz, Lect. Notes Phys. **828** 313, (2011); arXiv:1002.1722 [hep-th].
  - [8] R.G. Cai, L. Li, L.F. Li, and R.Q. Yang, Sci. China Phys. Mech. Astron. **58**, 060401 (2015); arXiv:1502.00437 [hep-th].
  - [9] S.A. Hartnoll, C.P. Herzog, and G.T. Horowitz, Phys. Rev. Lett. **101**, 031601 (2008).
  - [10] S.A. Hartnoll, C.P. Herzog, and G.T. Horowitz, J. High Energy Phys. **0812**, 015 (2008).
  - [11] S.S. Gubser and S.S. Pufu, J. High Energy Phys. **0811**, 033 (2008); arXiv:0805.2960 [hep-th].
  - [12] R.G. Cai, S. He, L. Li, and L.F. Li, J. High Energy Phys. **1312**, 036 (2013); arXiv:1309.2098 [hep-th].
  - [13] R.G. Cai, L. Li, and L.F. Li, J. High Energy Phys. **1401**, 032 (2014); arXiv:1309.4877 [hep-th].
  - [14] J.W. Chen, Y.J. Kao, D. Maity, W.Y. Wen, and C.P. Yeh, Phys. Rev. D **81**, 106008 (2010); arXiv: 1003.2991 [hep-th].
  - [15] F. Benini, C.P. Herzog, R. Rahman, and A. Yarom, J. High Energy Phys. **1011**, 137 (2010); arXiv: 1007.1981 [hep-th].
  - [16] P. Basu, A. Mukherjee, and H.H. Shieh, Phys. Rev. D **79**, 045010 (2009).
  - [17] C.P. Herzog, P.K. Kovtun, and D.T. Son, Phys. Rev. D **79**, 066002 (2009).
  - [18] D. Arean, P. Basu, and C. Krishnan, J. High Energy Phys. **1010**, 006 (2010).
  - [19] Y.B. Wu, J.W. Lu, W.X. Zhang, C.Y. Zhang, J.B. Lu, and F. Yu, Phys. Rev. D **90**, 126006 (2014); arXiv:1410.5243 [hep-th].
  - [20] Y.B. Wu, J.W. Lu, C.Y. Zhang, N. Zhang, X. Zhang, Z.Q. Yang, and S.Y. Wu, Phys. Lett. B **741**, 138 (2015); arXiv:1412.3689 [hep-th].
  - [21] D. Arean, M. Bertolini, J. Evslin, and T. Prochazka, J. High Energy Phys. **1007**, 060 (2010).
  - [22] J. Sonner and B. Withers, Phys. Rev. D **82**, 026001 (2010).
  - [23] H.B. Zeng, W.M. Sun, and H.S. Zong, Phys. Rev. D **83**, 046010 (2011).
  - [24] Y. Peng, X.M. Kuang, Y.Q. Liu, and B. Wang, arXiv:1204.2853 [hep-th].
  - [25] X.M. Kuang, Y.Q. Liu, and B. Wang, Phys. Rev. D **86**, 046008 (2012).
  - [26] I. Amado, D. Arean, A. Jimenez-Alba, K. Landsteiner, L. Melgar, and I.S. Landea, J. High Energy Phys. **1307**, 108 (2013).
  - [27] H.B. Zeng, Phys. Rev. D **87**, 046009 (2013).
  - [28] I. Amado, D. Arean, A. Jimenez-Alba, K. Landsteiner, L. Melgar, and I.S. Landea, J. High Energy Phys. **1402**, 063 (2014).
  - [29] C.Y. Lai, Q.Y. Pan, J.L. Jing, and Y.J. Wang, Phys. Lett. B **757**, 65 (2016); arXiv:1601.00134 [hep-th].
  - [30] R. Arias and I.S. Landea, arXiv:1608.01687 [hep-th].
  - [31] R.G. Cai, Phys. Rev. D **65**, 084014 (2002); arXiv:hep-th/0109133.
  - [32] R. Gregory, S. Kanno, and J. Soda, J. High Energy Phys. **0910**, 010 (2009).
  - [33] Q.Y. Pan, B. Wang, E. Papantonopoulos, J. Oliveria, and A.B. Pavan, Phys. Rev. D **81**, 106007 (2010).
  - [34] Q.Y. Pan and B. Wang, Phys. Lett. B **693**, 159 (2010).
  - [35] J.L. Jing, L.C. Wang, Q.Y. Pan, and S.B. Chen Phys. Rev. D **83**, 066010 (2011).
  - [36] X.H. Ge, B. Wang, S.F. Wu, and G.H. Yang, J. High Energy Phys. **1008**, 108 (2010); arXiv:1002.4901 [hep-th].
  - [37] Y. Brihaye and B. Hartmann, Phys. Rev. D **81**, 126008 (2010); arXiv:1003.5130 [hep-th].
  - [38] R.G. Cai, Z.Y. Nie, and H.Q. Zhang, Phys. Rev. D **82**, 066007 (2010); arXiv:1007.3321 [hep-th].
  - [39] L. Barclay, R. Gregory, S. Kanno, and P. Sutcliffe, J. High Energy Phys. **1012**, 029 (2010); arXiv:1009.1991 [hep-th].
  - [40] R. Gregory, J. Phys. Conf. Ser. **283**, 012016 (2011); arXiv:1012.1558 [hep-th].
  - [41] H.F. Li, R.G. Cai, and H.Q. Zhang, J. High Energy Phys. **1104**, 028 (2011).
  - [42] S. Kanno, Class. Quant. Grav. **28**, 127001 (2011).
  - [43] S. Gangopadhyay and D. Roychowdhury, J. High Energy Phys. **1205**, 156 (2012); **1208**, 104 (2012).
  - [44] W.P. Yao and J.L. Jing, J. High Energy Phys. **1305**, 101 (2013).
  - [45] Z.Y. Nie and H. Zeng J. High Energy Phys. **1510**, 047 (2015).
  - [46] D. Ghorai and S. Gangopadhyay, Eur. Phys. J. C **76**, 146 (2016).
  - [47] A. Sheykhi, H.R. Salahi, and A. Montakhab, J. High Energy Phys. **1604**, 058 (2016).
  - [48] H.R. Salahi, A. Sheykhi, and A. Montakhab, Eur. Phys. J. C **76**, 575 (2016); arXiv:1608.05025 [gr-qc].
  - [49] J.W. Lu, Y.B. Wu, T. Cai, H.M. Liu, Y.S. Ren, and M.L. Liu, Nucl. Phys. B **903**, 360 (2016).
  - [50] M. Brigante, H. Liu, R.C. Myers, S. Shenker and S. Yaida, Phys. Rev. Lett. **100**, 191601 (2008); arXiv:0802.3318 [hep-th].

- [51] A. Buchel and R.C. Myers, J. High Energy Phys. **0908**, 016 (2009); arXiv: 0906.2922 [hep-th].
- [52] M. Tinkham, Introduction to Superconductivity (McGrawHill, New York, 1996).